Thermal Enhancement and Quenching of Upconversion Emission in Nanocrystals

Zijun Wang,[1] Jeppe Christiansen,[2] Dennie Wezendonk,[3] Xiaobin Xie,[4] Marijn A. van Huis,[4] Andries Meijerink[1]*

[1] *Condensed Matter and Interfaces, Debye Institute for Nanomaterials Science, Utrecht University, Princetonplein 1, 3584 CC Utrecht, The Netherlands.*

[2] *Department of Physics and Astronomy, Aarhus University, Ny Munkegade 120, DK-8000 Aarhus C, Denmark.*

[3] *Inorganic Chemistry and Catalysis, Debye Institute for Nanomaterials Science, Utrecht University, Universiteitsweg 99, 3584 CG, Utrecht, The Netherlands.*

[4] *Soft Condensed Matter, Debye Institute for Nanomaterials Science, Utrecht University, Princetonplein 1, 3584 CC Utrecht, The Netherlands.*

*E-mail: A.Meijerink@uu.nl

EXPERIMENTAL SECTION

Chemicals The synthesis was conducted with commercially available reagents. Absolute ethanol (Analytical Reagent, A.R.), cyclohexane (A.R.), oleic acid (90%), oleylamine (80%-90%), 1-octadecene (90%), RE (III) acetate (RE = Y, Ho, Er, Tm and Yb, 99.9%), hexacarbonyl tungsten (97%), sodium hydroxide (A.R.), tungsten oxide (A.R.), sodium bicarbonate (A.R.) and RE oxide (RE = Y, Ho, Er, Tm and Yb, 99.99%) were purchased from Sigma and Aldrich without further purification.

Synthesis of tungstate NCs In a three-necked flask, oleic acid (10 mL), oleylamine (10 mL) and 1-octadecene (20 mL) were mixed with RE (III) acetate (1 mmol), hexacarbonyl tungsten (2 mmol) and sodium hydroxide (1.5 mmol) with stirring and heating at 390 K for 0.5 h. The reaction was heated to 570 K for 2 h while refluxing under a protective nitrogen atmosphere.

Once cooled to room temperature, the product was precipitated and washed with ethanol and cyclohexane for three times via centrifugation, then dried at 370 K overnight for the measurements.

Synthesis of tungstate bulk materials Microcrystalline samples with composition $NaY(WO_4)_2$:49Yb1RE (RE = Ho, Er and Tm) were prepared by solid state reaction. The stoichiometric raw materials of WO_3, $NaHCO_3$ and RE_2O_3 were ground in agate mortar and then transferred to alumina crucible. Subsequently, the mixture was first sintered at 773 K for 4 h and then at 1273 K for 4 h in oven with ambient atmosphere.

Characterization The photoluminescence spectra were recorded by an Edinburgh Instruments FLS920 spectrometer. For UC emission spectra, the excitation source and the detector were a 980 nm continuous wave laser (~1 W/cm^2) and a Hamamatsu R928 photomultiplier tube (PMT). The luminescence decay dynamics of Er^{3+} UC emission was measured with an Ekspla NT342B-10-SH/DUV OPO system for pulsed excitation (pulse width 5 ns and repetition rate 10 Hz) and a Hamamatsu H7422-02 PMT as photon detector with a Triax 550 monochromator coupled to a PicoQuant TimeHarp 260 photo-counting module at a discriminator level of -100 mV. The decay dynamics of Yb^{3+} IR emission was measured by using a liquid-nitrogen cooled Hamamatsu R5507-73 PMT and multi-channel scaling (MCS) option integrated in the Edinburgh spectrofluorometer. The pulsed excitation source was an optical parametric oscillator (OPO) system (410-2200 nm, Opotek Opolette HE 355 II) pumped by the third harmonic of a YAG:Nd^{3+} laser (~1 mJ pulses with a 10 ns pulse duration and repetition rate 20 Hz). To control the temperature, a Linkam THMS600 Microscope Stage was used for the temperature range of 300-600 K. The spectrum was collected at an interval of at least 10 minutes to guarantee the temperature stability for sample. The thermocouple allows for monitoring and compensation of IR laser heating effects. The relative humidity of air is 40-60%.

For the TEM measurements, NCs dropcasted on amorphous carbon-coated copper grids were imaged using an FEI Talos F200X TEM microscope operating at 200 kV. For the in-situ heating measurements, NCs were dropcasted on heating chips with SiN membranes, which were mounted on a DENSsolutions MEMS-based heating holder. For the ex-situ measurements, NCs were dropcasted on SiO-coated TEM grids and the prepared grids were sintered in oven at 600 K for 10 min. In-situ XRD measurements were performed on a Bruker5 AXS D8 X-ray diffractometer in combination with an Anton Paar XRK 900 reactor chamber

for Co Kα radiation with a wavelength of 1.79 Å and a VÅNTEC 1D position sensitive detector. FT-IR spectra were measured in air in a Vertex 70 (Bruker) spectrometer equipped with KBr/DLaTGS D301 detector using KBr pellet technique. The thermogravimetric analysis was performed on a Perkin Elmer TGA8000 with a temperature ramp from 300 to 570 K at 5 K/min in an atmosphere of 20% oxygen in argon.

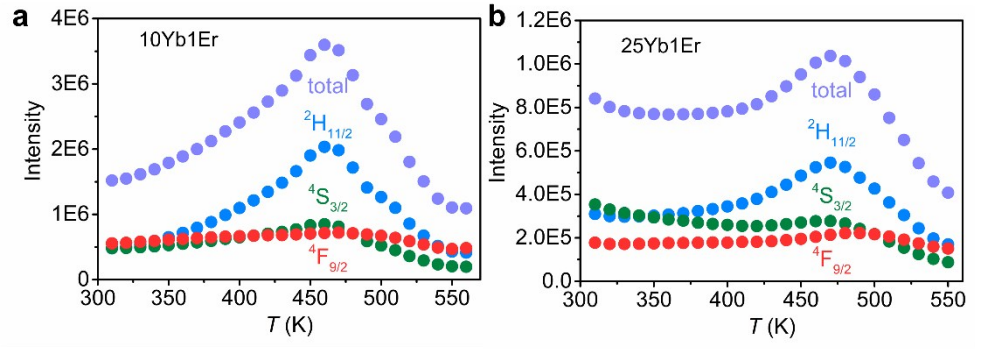

Figure S1. Temperature-dependent integrated intensity of Er^{3+} emission lines ($^2H_{11/2}$, $^4S_{3/2}$, $^4F_{9/2} \rightarrow {}^4I_{15/2}$ transitions and the sum) derived from emission spectra of 980 nm excitation for (a) $NaY(WO_4)_2$:10Yb1Er and (b) $NaY(WO_4)_2$:25Yb1Er NCs in air.

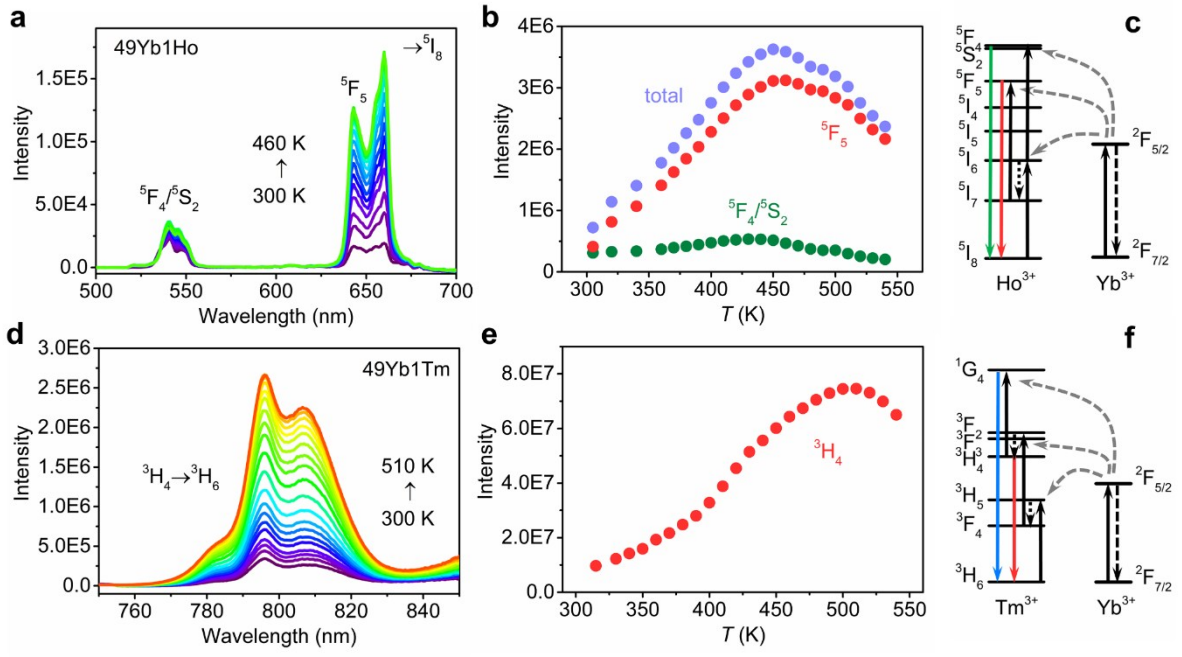

Figure S2. Temperature-dependent measurements for (a-c) $NaY(WO_4)_2$:49Yb1Ho and (d-f) $NaY(WO_4)_2$:49Yb1Tm NCs in air. (a, d) Emission spectra under pulsed 980 nm excitation. (b, e) Integrated intensity of Ho^{3+} emission lines ($^5F_4/^5S_2$, $^5F_5 \rightarrow {}^5I_8$ transitions and the sum) and

Tm^{3+} emission line ($^3H_4 \rightarrow {}^3H_6$ transition) for the emission spectra in (a, d). (c, f) Energy levels of Ho^{3+}-Yb^{3+} and Tm^{3+}-Yb^{3+} ion couples showing the UC processes.

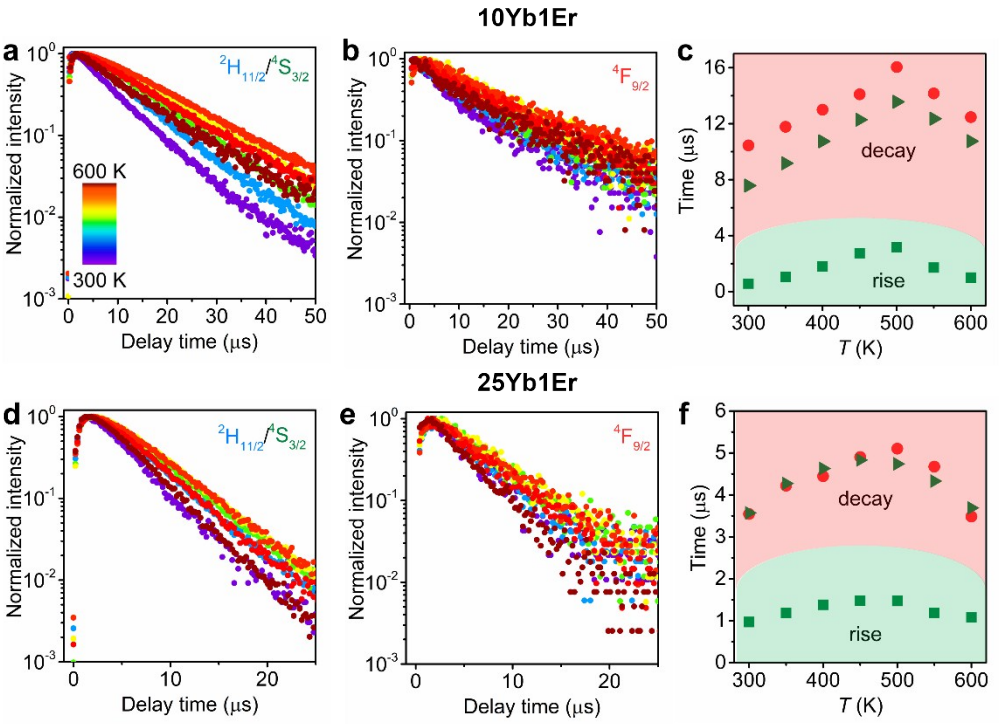

Figure S3. Temperature-dependent luminescence decay for (a-c) $NaY(WO_4)_2$:10Yb1Er and (d-f) $NaY(WO_4)_2$:25Yb1Er NCs in air under pulsed 980 nm excitation. Luminescence decay curves for (a, d) $^2H_{11/2}/^4S_{3/2}$ states and (b, e) $^4F_{9/2}$ state. (c, f) Decay times (green triangles for $^2H_{11/2}/^4S_{3/2}$ states and red circles for $^4F_{9/2}$ state) and rise time (green squares for $^2H_{11/2}/^4S_{3/2}$ states) determined from the decay curves in (a, b) and (d, e).

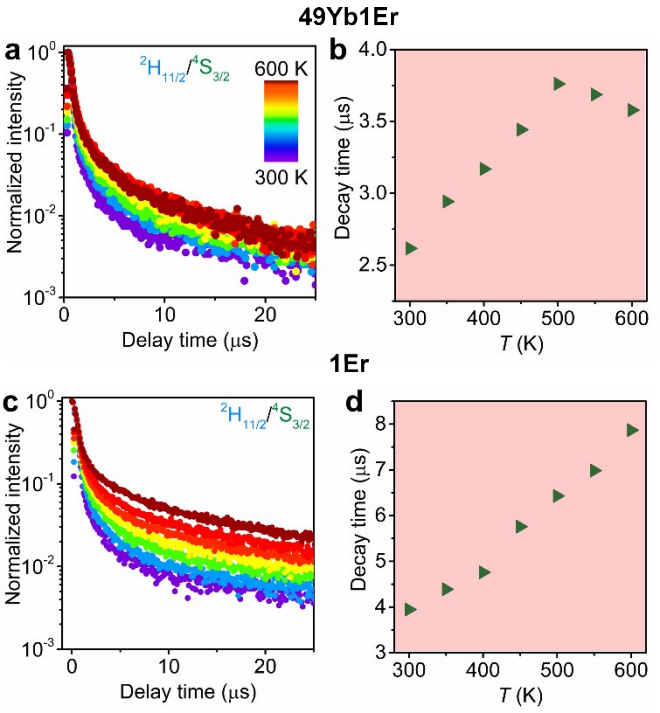

Figure S4. Temperature-dependent luminescence decay of $^2H_{11/2}/^4S_{3/2}$ states under pulsed 480 nm excitation for (a, b) $NaY(WO_4)_2$:49Yb1Er and (c, d) $NaY(WO_4)_2$:1Er NCs in air. (a, c) Luminescence decay curves. (b, d) Decay time.

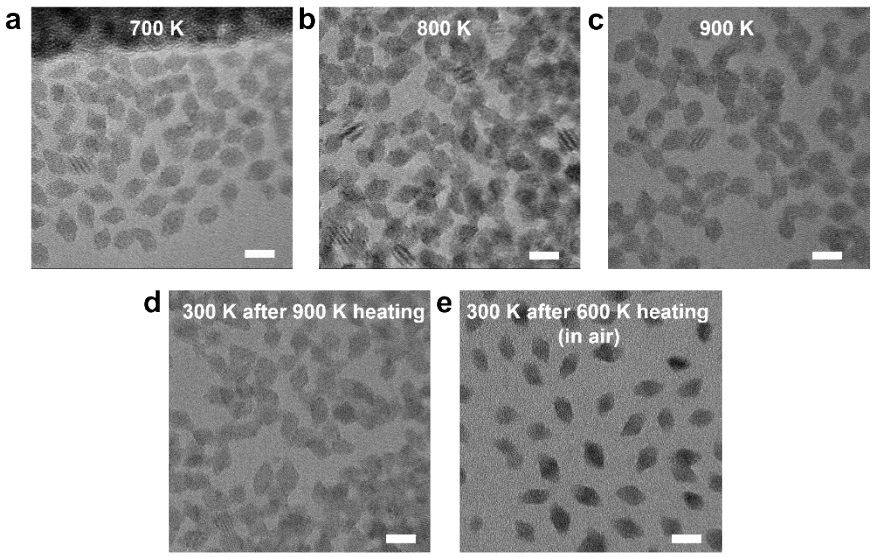

Figure S5. Bright-field TEM images of $NaY(WO_4)_2$:49Yb1Er NCs recorded at various temperatures during in-situ heating at (a) 700, (b) 800, and (c) 900 K, and (d) after subsequent cooling to 300 K. (e) Bright-field TEM images recorded at 300 K after ex-situ heating in an oven in air at 600 K for 10 min. (scale bar = 10 nm)

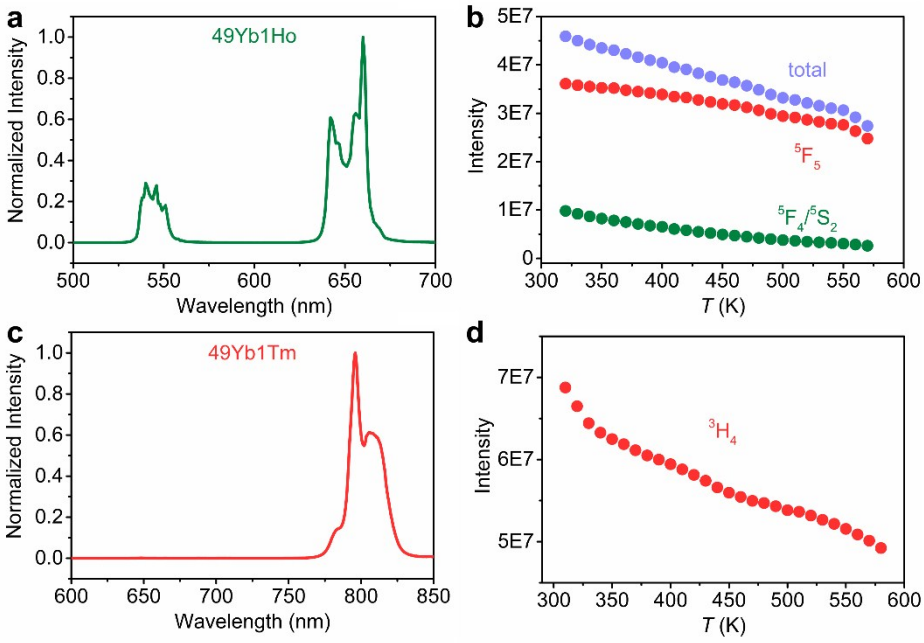

Figure S6. Temperature-dependent luminescence of $NaY(WO_4)_2$:49Yb1Ho and $NaY(WO_4)_2$:49Yb1Tm bulk materials in air under 980 nm excitation. (a) Emission spectrum at 300 K for Ho^{3+}-doped sample. (b) Integrated intensity of Ho^{3+} emission lines ($^5F_4/^5S_2$, $^5F_5$ → $^5I_8$ transitions and the sum) for emission spectra. (c) Emission spectrum at 300 K for Tm^{3+}-doped sample. (d) Integrated intensity of Tm^{3+} emission line ($^3H_4$ → $^3H_6$ transition) for emission spectra.

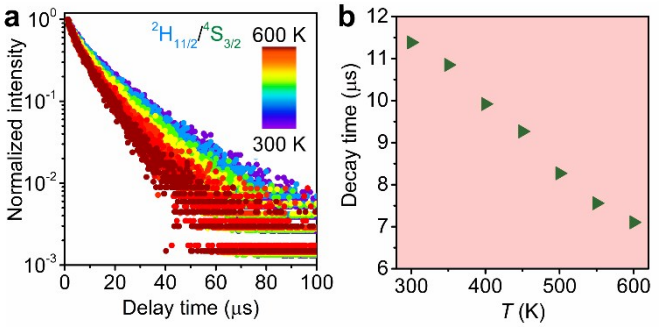

Figure S7. Temperature-dependent luminescence (a) decay curves and (b) decay time of $^2H_{11/2}/^4S_{3/2}$ states for $NaY(WO_4)_2$:49Yb1Er bulk materials in air under pulsed 480 nm excitation.

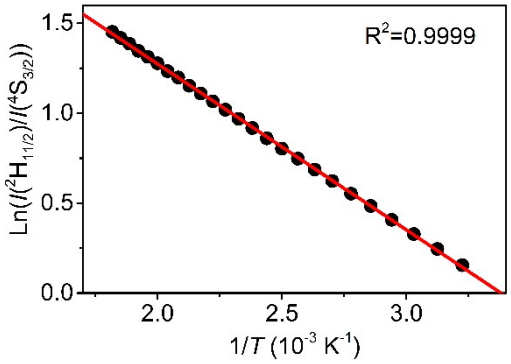

Figure S8. The linear relation between the natural logarithm of the integrated intensity ratio of the $^2H_{11/2}$ and $^4S_{3/2}$ emission lines ($I(^2H_{11/2}/^4S_{3/2})$) and the inverse of temperature T for $NaY(WO_4)_2$:49Yb1Er bulk materials in air. The data are fitted by $I(^2H_{11/2}/^4S_{3/2}) = A \exp(-\Delta E/(KT))$, where A is a constant, ΔE is energy separation of $^2H_{11/2}$ and $^4S_{3/2}$ levels, and K is Boltzmann constant.

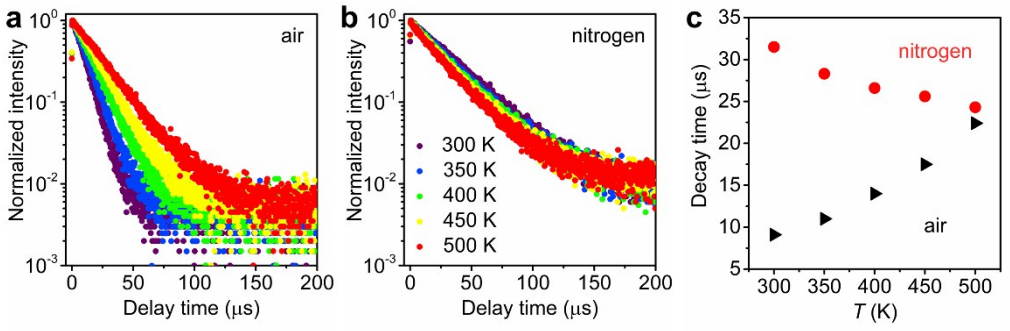

Figure S9. Temperature-dependent luminescence (a, b) decay curves and (c) decay time of Yb^{3+} 980 nm emission for $NaY(WO_4)_2$:49Yb NCs in (a) air and (b) dry nitrogen under pulsed 960 nm excitation.

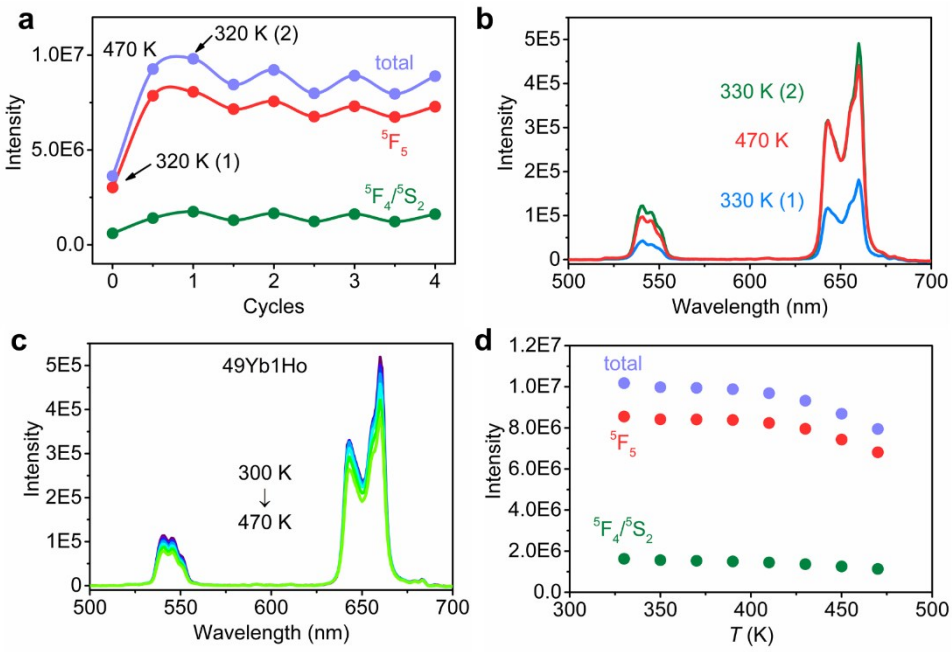

Figure S10. Temperature-dependent luminescence of $NaY(WO_4)_2$:49Yb1Ho NCs in nitrogen under 980 nm excitation. (a) Cycling experiment for integrated intensity of Ho^{3+} emission lines ($^5F_4/^5S_2$, $^5F_5 \rightarrow {}^5I_8$ transitions and the sum). (b) Emission spectra for the first three temperature points in cycling experiment. (c) Temperature-dependent emission spectra for NCs after first cycle of heating and cooling. (b) Integrated intensity of Ho^{3+} emission lines ($^5F_4/^5S_2$, $^5F_5 \rightarrow {}^5I_8$ transitions and the sum) for the emission spectra in (c).

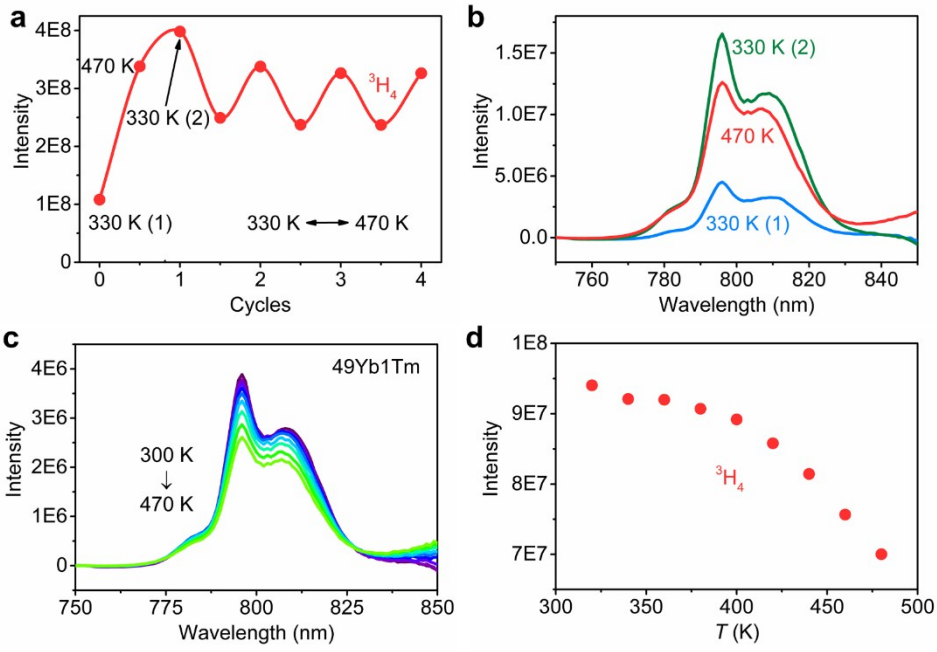

Figure S11. Temperature-dependent luminescence of $NaY(WO_4)_2$:49Yb1Tm NCs in nitrogen under 980 nm excitation. (a) Cycling experiment for integrated intensity of Tm^{3+} emission line ($^3H_4 \rightarrow {}^3H_6$ transition). (b) Emission spectra for the first three temperature points in cycling experiment. (c) Temperature-dependent emission spectra for NCs after first cycle of heating and cooling. (b) Integrated intensity of Tm^{3+} emission line ($^3H_4 \rightarrow {}^3H_6$ transition) for the emission spectra in (c).

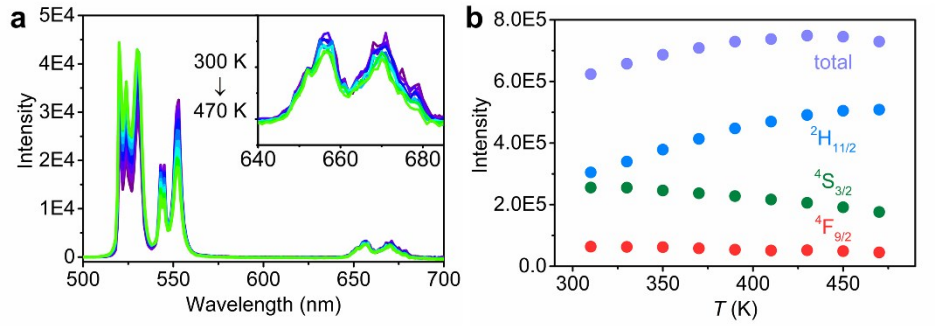

Figure S12. Temperature-dependent luminescence of $NaY(WO_4)_2$:49Yb1Er bulk material in nitrogen under 980 nm excitation. (a) Temperature-dependent emission spectra for sample after first cycle of heating and cooling. (b) Integrated intensity of Er^{3+} emission lines ($^2H_{11/2}$, $^4S_{3/2}$, $^4F_{9/2} \rightarrow {}^4I_{15/2}$ transitions and the sum) for the emission spectra in (a).

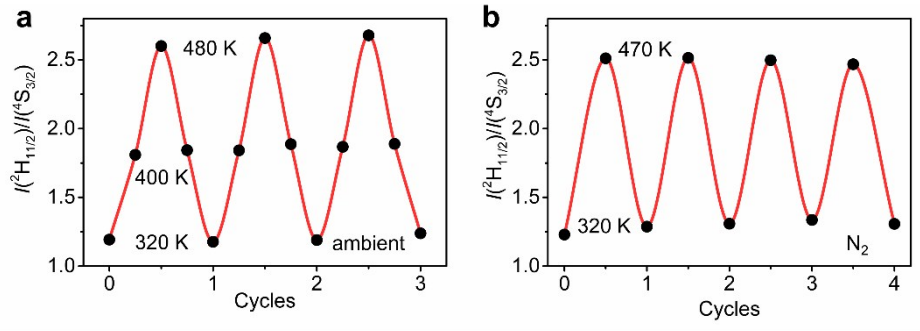

Figure S13. Cycling experiment for Er^{3+} emission intensity ratio of $^2H_{11/2}/^4S_{3/2}$ derived from emission spectra of 980 nm excitation for $NaY(WO_4)_2$:49Yb1Er NCs in (a) air and (b) dry nitrogen.